Fiber-Coupled Diamond Quantum Nanophotonic Interface

Michael J. Burek, Charles Meuwly, Ruffin E. Evans, Mihir K. Bhaskar, Alp Sipahigil, Srujan Meesala, Bartholomeus Machielse, Denis D. Sukachev, Christian T. Nguyen, Jose L. Pacheco, Edward Bielejec, Mikhail D. Lukin, and Marko Lončar

Phys. Rev. Applied **8**, 024026 — Published 25 August 2017

DOI: 10.1103/PhysRevApplied.8.024026

A FIBER-COUPLED DIAMOND QUANTUM NANOPHOTONIC INTERFACE

Michael J. Burek[a], Charles Meuwly[a,b], Ruffin E. Evans[c], Mihir K. Bhaskar[c], Alp Sipahigil[c], Srujan Meesala[a], Bartholomeus Machielse[c], Denis D. Sukachev[c,d,e], Christian T. Nguyen[c], Jose L. Pacheco[e], Edward Bielejec[e], Mikhail D. Lukin[c], and Marko Lončar[a,†]

[a.] John A. Paulson School of Engineering and Applied Sciences, Harvard University, 29 Oxford Street, Cambridge, MA 02138, USA

[b.] École Polytechnique Fédérale de Lausanne (EPFL), CH-1015 Lausanne, Switzerland

[c.] Department of Physics, Harvard University, 17 Oxford Street, Cambridge, MA 02138, USA

[d.] P. N. Lebedev Physical Institute of the RAS, Moscow 119991, Russia

[e.] Russian Quantum Center, Skolkovo, Moscow 143025, Russia

[f.] Sandia National Laboratories, Albuquerque, NM 87185, USA

[†] Corresponding author contact: E-mail: loncar@seas.harvard.edu. Tel: (617) 495-579. Fax: (617) 496-6404.

ABSTRACT – Color centers in diamond provide a promising platform for quantum optics in the solid state, with coherent optical transitions and long-lived electron and nuclear spins. Building upon recent demonstrations of nanophotonic waveguides and optical cavities in single-crystal diamond, we now demonstrate on-chip diamond nanophotonics with a high efficiency fiber-optical interface, achieving > 90% power coupling at visible wavelengths. We use this approach to demonstrate a bright source of narrowband single photons, based on a silicon-vacancy color center embedded within a waveguide-coupled diamond photonic crystal cavity. Our fiber-coupled diamond quantum nanophotonic interface results in a high flux (~ 38 kHz) of coherent single photons (near Fourier-limited at < 1 GHz bandwidth), into a single mode fiber, enabling new possibilities for realizing quantum networks that interface multiple emitters, both on-chip and separated by long distances.

I. INTRODUCTION

Luminescent point defects ("color centers") in diamond provide a solid-state platform for the realization of scalable quantum technologies [1]. For instance, demonstrations that leverage the nitrogen vacancy (NV) center in diamond as a spin-photon interface [2-7], have included the entanglement of two distant solid-state qubits [8] and long-distance quantum teleportation [9]. While such advances have enabled recent tests of fundamental laws of nature [10], entanglement generation rates in these experiments are currently limited by the rate of coherent photon generation and collection. To develop a scalable architecture for the realization of quantum networks [11, 12], it will ultimately be necessary to engineer efficient single-photon emission into well-defined spatio-temporal modes [13].

Towards this goal, parallel efforts in the field of diamond nanofabrication and nanophotonics, have demonstrated on-chip low loss (~ db/cm) diamond waveguides and a wide range of high quality (Q) factor optical cavities [12, 14-26]. Recently, angled-etching nanofabrication [27-30] has emerged as a scalable method for realizing nanophotonic devices from bulk single-crystal diamond substrates. Using this approach, we have demonstrated high Q-factor ($> 10^5$) diamond photonic crystal cavities (PCCs) [31] operating over a wide wavelength range (visible to telecom). Monolithic diamond PCCs fabricated by angled-etching are especially attractive for their compatibility with post-fabrication processing techniques necessary to stabilize implantation-defined color centers, i.e. high temperature annealing and acid treatments [32, 33]. Together, recent efforts in quantum science and nanoscale engineering of diamond have resulted in the demonstration of a solid-state single-photon switch based on a single silicon-vacancy (SiV) color center embedded in a diamond PCC, as well as observation of entanglement between two SiVs implanted in a single diamond waveguide [12]. As diamond nanophotonics continues to enable advances in other disciplines (including non-linear optics [34, 35] and optomechanics [36,

37]), the demand for scalable technology necessitates moving beyond isolated devices, to fully integrated on-chip nanophotonic networks in which waveguides route photons between optical cavities [38]. Moreover, for applications involving single photons, such as quantum nonlinear optics with diamond color centers [12, 22], efficient off-chip optical coupling schemes are necessary to provide seamless transition of on-chip photons into commercial single mode optical fibers [39-42].

Herein, we demonstrate on-chip diamond nanophotonics integrated with a high efficiency fiber-optical interface, achieving greater than 90% power coupling at visible wavelengths. Our diamond nanophotonic structures utilize free-standing angled-etched waveguides (Figure 1), which retain low optical loss despite being physically supported through attachment to the bulk substrate [43], and are able to efficiently route photons on-chip [31]. The fiber-optical coupling scheme utilizes a single mode optical fiber, with one end chemically etched into a conical taper, to adiabatically transition guided light between on-chip diamond waveguides and off-chip optical fiber networks. Finally, we use our fiber-coupled diamond nanophotonics platform to demonstrate a bright source of narrowband single photons (near Fourier-limited at < 1 GHz bandwidth), based on a SiV center embedded within a waveguide-coupled diamond PCC. We achieve a coherent single photon generation rate of ~ 38 kHz, representing nearly an order of magnitude improvement compared to previous demonstrations of coherent zero-phonon-line (ZPL) photons collected from a single color center in diamond [5, 6, 44], with the additional advantage of providing these photons in a single-mode optical fiber. Our work will ultimately enable new possibilities for realizing quantum networks that interface multiple emitters, both on-chip and separated by long distances.

II. ON-CHIP DIAMOND NANOPHOTONIC STRUCTURES

Figure 1 displays a series of SEM images revealing diamond nanophotonic structures realized by angled-etching nanofabrication [27, 28] (see Supplementary Material for more details [45]). The nanophotonic systems consist of four key components: (1) freestanding diamond waveguides, (2) waveguide-coupled diamond nanobeam photonic crystal cavities (PCCs, Figure 1 (b)), (3) vertical waveguide support structures (Figure 1 (c)), and lastly, (4) freestanding diamond waveguide tapers (DWTs, Figure 1 (d) and (e)).

A. DIAMOND NANOBEAM PHOTONIC CRYSTAL CAVITIES

PCCs enable high optical Q-factors while retaining wavelength-scale mode volumes [46], a key ingredient enabling strong light-matter interactions [11, 13]. Additionally, diamond nanobeam PCCs (see Figure 1 (b) inset and Ref. [45] for additional details) are readily integrated with on-chip waveguides, as the cavity architecture is naturally built into a suspended waveguide segment. This makes it possible to engineer waveguide-damped cavities where decay into the waveguide is much larger than scattering and absorption losses [47, 48]. We target the diamond PCC design used in this work to support a fundamental cavity mode resonance near $\lambda \sim 737$ nm, corresponding to the optical transition of the SiV center [49, 50]. Additionally, we focus on transverse-electric (TE) polarized cavity modes, which have their major electric field component mostly perpendicular to the $y = 0$ plane (see Figure 1 (b) inset for coordinate convention). From finite difference time domain (FDTD) electromagnetic simulations, the cavity mode volume was $V_{mode} \sim 0.52\ (\lambda /n)^3$, where n is the diamond refractive index, a four-fold improvement compared with our previous results for diamond PCCs fabricated in bulk diamond [12], and a two-fold improvement over other state-of-the-art systems [21]. For fabricated structures, the number of Bragg mirror segments included in the nanobeam cavity was set

to fix the total Q-factor of the device (as confirmed by FDTD simulations) to $Q_{total} \sim 10^4$, with cavity losses dominated by coupling to the feeding waveguide (intrinsic radiative losses were estimated to be $Q_{rad} \sim 2 \times 10^5$ by FDTD simulations). Additionally, to limit insertion (scattering) losses into the cavity, several holes that reduce quadratically in pitch and radii were appended to the ends of the PCC to ensure an adiabatic transition between the waveguide mode and Bloch mode of the Bragg mirror [51].

B. VERTICAL WAVEGUIDE SUPPORT STRUCTURES

Freestanding waveguides and PCCs realized by angled-etching ultimately require physical support through attachment to the bulk diamond substrate. To ensure robust mechanical performance while minimizing optical transmission loss, we employ vertical waveguide support structures [43], created by increasing the waveguide width by approximately 30 % of the nominal value and gradually tapering over 10 μm long straight portions (Figure 1 (c)). With angled-etching nanofabrication, wider waveguide sections require longer etch times to fully release from the bulk substrate. Consequently, wider waveguide sections remain attached to the substrate, resulting in a pedestal-like cross-section [31, 43]. At the same time, the adiabatically tapered support along the waveguide path minimizes optical transmission losses through the structure. From SEM images, we estimate the thickness of the diamond material supporting the widest portion of the waveguide (mid-support) to be < 100 nm, with prior measurements of transmission losses through such fabricated structures to be on order $\sim 10^{-3}$ dB per support [31].

C. DIAMOND WAVEGUIDE TAPERS

To efficiently couple light from our diamond nanophotonic structures, we adapt a fiber-optical interface previously developed for suspended silicon nitride nanophotonic systems [39]. Specifically, we employ a single-ended conical optical fiber taper (OFT, described in the following section) to make physical contact between the OFT tip and the on-chip freestanding DWT (Figure 1 (e)). Freestanding DWTs gradually change the effective refractive index of the waveguide mode along the propagation direction, such that nearly all optical power remains in the target eigenmode. To minimize coupling to higher-order modes, we exploit gradual tapering which fulfills the adiabatic condition [39]: $dn_{wvg}/dx < (2\pi/\lambda)\left|n_{eff,1}(x) - n_{eff,2}(x)\right|^2$, where n_{wvg} is the effective index of the diamond waveguide, $n_{\mathrm{eff,i}}$ is the effective index of the i^{th} waveguide mode along the taper, and λ = 737 nm is the free-space wavelength. Freestanding DWTs were designed to evolve from the nominal diamond waveguide width (~ 500 nm) down to a sub < 50 nm point, over a 20 μm length, yielding a final taper angle of ~ 2^{o}. We note that the DWTs scale in all three dimensions as a result of angled-etching nanofabrication, since the waveguide width defines its thickness via a constant etch angle [27].

III. EFFICIENT OPTICAL FIBER TAPER COUPLING

A. SIMULATION OF COUPLING EFFICIENCY

In the region of physical contact between the DWT and OFT (schematically represented in Figure 2 (a)), propagating guided modes couple via their evanescent fields, forming a hybridized "supermode" [39]. Figure 2(b) displays the calculated effective indices of a DWT physically coupled to a single-ended OFT (insets display cross-sectional eigenmode profiles obtained from simulation). With this geometry, the latter has n_{eff} greater than ~ 1.28 over the entire length of the coupler, indicating that the optical

mode remains well confined throughout the DWT-OFT structure. To confirm adiabatic mode transfer, we employ FDTD simulations to launch a propagating fundamental TE polarized mode down the diamond waveguide (Figure 2(c)), and monitor the power output in the HE_{11} optical fiber mode after the coupling region. A power transfer of ~ 98 % is achieved for a 20 μm contact region (equal to the DWT length), corresponding to a coupling loss of less than 0.09 dB per facet. High efficiency coupling is also observed as the OFT overlap with the DWT is increased up to nearly 50 μm (Figure 2 (c)), while the DWT length is maintained at 20 μm.

B. OPTICAL FIBER TAPER FABRICATION

Single-ended conical OFTs were fabricated by a wet etching technique, where commercial near-infrared single-mode optical fibers (Thorlabs S630-HP) were submerged in hydrofluoric acid (HF) to form the taper profile [52], as depicted in Figure 2(d). A layer of o-xylene was added on top of the HF to promote gradual taper formation via an oil/water interface meniscus that wicks up the length of the fiber. As the etch progresses and the fiber diameter shrinks, the height of the oil/water interface meniscus naturally decreases, resulting in a tapered fiber diameter over a length defined by the etch rate and initial fiber diameter. When the acid etches completely through the fiber diameter, the OFT self-terminates. Drawing the fiber out of the HF solution at a fixed rate further extends the taper length, enabling full control over the final taper angle. Moreover, this etching protocol readily extends to the simultaneous fabrication of many nominally identical OFTs. For OFT angles less than ~ 4^{o}, the HE_{11} fiber mode adiabatically transitions over the entire length of the OFT (on order ~ 10 mm) [39]. Figure 2(d) shows a SEM image of a representative OFT tip fabricated by HF etching, with a final taper angle of ~ 1.5^{o}. Here, the significant surface roughness of the etched OFT (Figure 2 (e)) is a result of initial surface topography of the original commercial fiber [45]. However, the total distance over which the optical

mode evanescently leaks outside of the OFT tip is less than ~ 100 μm. Thus, scattering losses due to fiber roughness were not detrimental to the final coupling efficiency.

C. Optical characterization of diamond nanophotonic structures

The generalized optical fiber network used to collect reflection spectra from the waveguide-coupled diamond PCCs is shown in Figure 3 (a). Motorized stages precisely controlled the position of the single-ended OFT to bring it into physical contact with the DWT. A white-light laser source (NKT Photonics EXW-12) was coupled into the fiber network and launched into a 2x2 90:10 fiber coupler, with 90% of reflected light returned to the detection path. The transmitted source light polarization was adjusted with an inline fiber polarization controller (FPC, Thorlabs FPC030 loaded with S630-HP optical fiber to ensure preferential coupling to the fundamental TE-polarized diamond waveguide mode and TE-polarized diamond PCC resonances. Specifically, the diamond waveguide and PCC also support transverse magnetic (TM) polarized modes, which spectrally overlap with the TE-polarized modes of interest. For our particular PCC design, a TM passband (high transmission, low reflection) exists in the spectral region associated with the TE stopband (high reflection) and TE-polarized PCC resonances [45]. To avoid leakage of input laser light through coupling to TM polarized modes, the FPC was adjusted to maximize reflected laser light in the spectral vicinity of the fundamental TE polarized PCC resonance. Finally, an optical spectrum analyzer (OSA) recorded reflection spectra. For a qualitative estimate of coupling efficiency over a broad wavelength range, the diamond PCC under test was replaced with a commercial fiber-coupled retroreflector (FR-63, Silicon Lightwave Technology, Inc.).

Figure 3(b) displays an optical micrograph of the on-chip diamond nanophotonic network coupled to the OFT tip with the source white light laser turned on. Light readily couples through the optical fiber taper tip to the on-chip diamond waveguide, with the diamond PCC acting as a mirror for almost the

entire visible emission band. Light passed by the diamond photonic crystal cavity is scattered at the end of the diamond waveguide by an intentionally placed notch in the waveguide. A broadband reflection spectrum collected from a representative diamond PCC (Figure 3 (c), blue curve), exhibits a series of reflection dips attributed to localized TE-polarized cavity resonances, and demonstrates the broadband nature (over 200 nm) of this OFT-DWT coupling approach. A high-resolution spectrum of the fundamental diamond PCC mode at 733.9 nm (indicated by the green circle) is shown in Figure 3 (d), with a Lorentzian fit to the spectra yielding a Q-factor of ~ 1.1 x 10^4. The on-resonance normalized reflection is ~ 46%, which give an estimate of the Q-factor due to radiative losses or absorption of ~ 3.4 x 10^4 [48]. Higher order longitudinal modes of the cavity are strongly waveguide damped, the second order diamond PCC resonance a λ ~ 780 nm has Q ~ 1.2 x 10^3). We find good agreement between the distribution of observed cavity resonances compared to design parameters (details provided in [45]), with a > 30 % overall yield of PCC devices suitable for experiments described in Section 4.

Away from the localized cavity resonances, we assume the diamond PCC ideally reflects all the TE-polarized light coupled to the diamond waveguide, allowing for an accurate calculation of the coupling efficiency. The off-resonant input power (P_{in}) and the reflected powers after the 2x2 coupler (P_r) are measured with a calibrated power meter. The normalized reflection is thus given by $P_r / P_{in} = \eta_c^2 \eta_{BS} \eta_m \eta_{FC}$, where η_c is the OFT-DWT coupling efficiency, η_{BS} is the calibrated coupling ratio of the 2x2 fiber coupler, η_m is the reflection of the nanobeam cavity Bragg mirror (assumed to be ~ 1), and η_{FC} ~ 92 % is the coupling efficiency of the FC-FC fiber coupler. Neglecting other losses in the diamond waveguide, we estimate a coupling efficiency η_c ~ 91 % (measured with a pigtailed laser diode operating at wavelength of ~ 705 nm). We carried out a series of similar measurements [45] on waveguide-coupled diamond PCCs fabricated for operation at telecom wavelengths (~ 1480 to 1680 nm). Here, a maximum measured coupling efficiency of ~ 96 %, demonstrates the broadband nature of both diamond nanophotonics and this adiabatic OFT-DWT coupling scheme.

IV. EFFICIENT GENERATION AND COLLECTION OF NARROWBAND SINGLE PHOTONS

We utilize our described diamond nanophotonic structures to implement a bright source of narrowband single photons suitable for use in quantum information protocols. SiV color centers are embedded at the center of waveguide-coupled diamond PCCs via focused ion beam (FIB) implantation [12, 53, 54] followed by high temperature annealing [45]. Targeted implantation of Si^+ ions by FIB enables positioning of emitters within the PCC with ~ 40 nm precision in all three dimensions, and control over the average number of implanted ions. Substrates in this work include ~ 100 diamond PCCs, each resulting in a suitable SiV-cavity node with accurate spatial alignment. While the conversion yield of implanted Si+ ions to SiV emitters is ~ 1 to 2 %, we implant an several hundred ions in each PCC, resulting in several emitters which can be spectrally resolved (due to the native degree of inhomogeneous distribution of ZPL lines [12]). Therefore, the emitter creation step of our fabrication process is nearly deterministic, with near unity yield of SiV-cavity nodes suitable for experiments described below.

SiV centers are excited from free space using a scanning confocal microscope [12]. Fluorescence is detected in the waveguide using the fiber-coupled interface (depicted in Figure 4(a)). In order to isolate narrow optical transitions, we cool the device to a temperature of ~ 5 K within a liquid helium continuous flow cryostat, at which an optical Λ-system formed by the SiV spin-orbit eigenstates is accessible (Figure 4 (b), left inset) [49, 50]. We use resonant excitation on the $|u\rangle$ to $|e\rangle$ branch to generate Raman fluorescence on the $|e\rangle$ to $|c\rangle$ transition. One benefit of this scheme is that, by tuning the frequency of the driving laser, the frequency of the emitted photons can be tuned by more than 10

GHz [12]. We selectively collect this spectral component of the fluorescence using a home-built Fabry-Perot (FP) cavity (finesse ~ 100) as a filter. The intrinsic linewidth of the FP cavity, as measured by a tunable laser, was 1.37 +/- 0.05 GHz. This value corresponds to the mean of multiple measurements, where the quoted error represents one standard deviation. By scanning the FP cavity center frequency across the $|e\rangle$ to $|c\rangle$ transition, we measure an upper bound on the linewidth of collected photons of 1.27 ± 0.2 GHz, set by the FP cavity (Figure 4(b)). This value also represents the mean of all the individual linewidth measurements and its standard deviation. Given that the linewidth of the SiV Raman fluorescence through the FP cavity is within statistical error of the intrinsic FP cavity linewidth, we conclude the collected photons are near-Fourier limited with bandwidth significantly less than 1 GHz. Note that the bandwidth of the photons in this Raman scheme is fundamentally limited only by the coherence time of the spin-orbit ground states of the SiV, not the SiV excited-state lifetime [12, 55]

With the FP cavity fixed on resonance with the $|e\rangle$ to $|c\rangle$ transition, we measure the saturation of Raman fluorescence (Figure 4(c)) when the PCC is tuned onto resonance with the $|e\rangle$ to $|c\rangle$ transition. Here κ, the PCC linewidth measured via a tunable laser is approximately 39 GHz ($Q \sim 10^4$). Tuning of the PCC resonance is achieved via controlled condensation of an inert gas onto the device [12]. We measure a maximum Raman photon detection rate of ~ 38 kHz of when the PCC is on resonance. The fluorescence consists of single photons, as confirmed by anti-bunching in a fluorescence autocorrelation measurement (Figure 4(c), right inset). The non-ideal $g^2(0)$ value at zero time delay is attributed primarily to leakage of the excitation laser light through the FP cavity, as well as laser-induced background fluorescence. We note that the correlation time of the SiV Raman fluorescence is limited here by a combination of the optical pumping rate and the orbital relaxation time (on order ~ 10 ns) [12, 55], and not the SiV excited state lifetime (~ 1.7 ns).

Our cavity-coupled, coherent photon generation rate represents a significant improvement over the state of the art, when compared against previous demonstrations of coherent ZPL photons collected from

a single diamond color center. The spectral purity (< 1 GHz bandwidth) of our collected photons is an essential element of schemes requiring indistinguishable photons, including entanglement generation (the rate of which is typically proportional to the square of the photon generation rate [8]). Our work represents a significant improvement over the state of the art for narrow-band photon generation using color centers in diamond, where collection rates for spectrally pure ZPL photons from an individual SiV center [44] or NV center [5, 6] of only ~ 6 kHz and 0.2 – 1.1 kHz were observed, respectively.

Our photon detection rate is limited primarily by finite transmission through the FP cavity filter and related free-space optics (~ 11% transmission) after collection into the OFT. Accounting for these losses, we estimate a lower bound on the collection rate of unfiltered single photons to be ~ 0.45MHz in the single-mode optical fiber. Additionally, in the case of the particular Si^+ ion implanted diamond PCC device measured, the OFT-DWT coupling efficiency was limited to approximately 22 to 25%, primarily due to mechanical failure of the specific DWTs used in this experiment, and the limited degrees of freedom available for accurate fiber positioning in our cryogenic apparatus. We note that the observed mode of failure was a "snapping down" of the DWT into the diamond substrate, which can occur if the sample is air-dried out of a solvent. However, sufficient coupling (> 10 % efficiency) between the OFT and snapped down DWTs was observed for all devices investigated, giving a near unity yield for functional DWT creation, with some reaching coupling efficiencies near ~ 40 %. While this OFT-DWT coupling efficiency is less than what we have observed in ambient conditions, typical collection efficiencies into a single-mode fiber are < 10 % even in the best-case scenario of a high-NA objective and a solid immersion lens (SIL) machined into the diamond substrate [9], and typically < 1 %. While recent demonstrations of engineered diamond thin film gratings (such as bullseye designs [56]) have reported substantially improved photon collection from embedded color centers in bulk systems, our diamond quantum nanophotonic interface provides the additional benefit of an emitter coupled to a well confined optical mode [12].

Mitigating our current issues with improved post-fabrication sample processing and cryogenic OFT-coupling techniques, we expected to increase our detection rate of spectrally filtered ZPL photons beyond the ~ 100 kHz limit, assuming similar transmission losses through the FP cavity filter. Finally, in this continuous-driving Raman scheme, the ultimate limit to the single-photon emission rate is determined by the phonon-limited relaxation time (~ 40 ns) [55] between the ground states, which is required to reset population into $|u\rangle$ after emission of a Raman photon. In the future, this may be overcome in a pulsed excitation scheme in which the SiV is optically initialized in the state $|u\rangle$ before the Raman excitation pulse is applied.

V. CONCLUSIONS

In summary, we demonstrate on-chip diamond nanophotonic structures with a high efficiency fiber-optical interface, achieving > 90% power coupling at visible wavelengths. Our diamond nanophotonic networks utilize freestanding angled-etched waveguides, which retain low optical loss despite being physically supported through attachment to the bulk substrate, and are able to efficiently route photons on-chip. The fiber-optical coupling utilizes a single mode optical fiber, with one end chemically etched into a conical taper, to adiabatically transition guided light between on-chip diamond waveguides and off-chip optical fiber networks. With a SiV center embedded within our waveguide-coupled diamond PCC, we demonstrate a ~ 38 kHz flux of spectrally narrow single photons (< 1 GHz bandwidth), efficiently coupled to single-mode optical fiber. Our bright and narrowband fiber-integrated diamond nanophotonic quantum node is of immediate technological significance to applications in quantum optics [12]. Combined with advances in quantum control of the diamond SiV center [57-59] and

schemes for improved spin coherence times [55], this platform opens up new possibilities for realizing large-scale systems involving multiple emitters strongly interacting via photons [11, 13].

ACKNOWLEDGEMENTS

The authors acknowledge V. Venkataraman for useful discussion in the course of preparing this report and D. Perry for performing the focused ion beam implantation. This work was supported in part by the AFOSR Quantum Memories MURI (grant FA9550-12-1-0025), ONR MURI on Quantum Optomechanics (Grant No. N00014-15-1-2761), NSF QOP (grant PHY-0969816), NSF CUA (grant PHY-1125846), NSF EFRI ACQUIRE (award no. 5710004174), and the STC Center for Integrated Quantum Materials (NSF Grant No. DMR-1231319). Ion implantation was performed with support from the Laboratory Directed Research and Development Program and the Center for Integrated Nanotechnologies at Sandia National Laboratories, an Office of Science facility operated for the DOE (contract DE-AC04-94AL85000) by Sandia Corporation, a Lockheed Martin subsidiary. Device fabrication was performed in part at the Center for Nanoscale Systems (CNS), a member of the National Nanotechnology Infrastructure Network (NNIN), which is supported by the National Science Foundation under NSF award no. ECS-0335765. CNS is part of Harvard University.

REFERENCES

1. I. Aharonovich and E. Neu, Diamond Nanophotonics, Advanced Optical Materials, **2**, 911 (2014).
2. E. Togan, Y. Chu, A.S. Trifonov, L. Jiang, J. Maze, L. Childress, M.V.G. Dutt, A.S. Sorensen, P.R. Hemmer, A.S. Zibrov, and M.D. Lukin, Quantum entanglement between an optical photon and a solid-state spin qubit, Nature, **466**, 730 (2010).
3. L. Childress, M.V. Gurudev Dutt, J.M. Taylor, A.S. Zibrov, F. Jelezko, J. Wrachtrup, P.R. Hemmer, and M.D. Lukin, Coherent Dynamics of Coupled Electron and Nuclear Spin Qubits in Diamond, Science, **314**, 281 (2006).
4. M.V.G. Dutt, L. Childress, L. Jiang, E. Togan, J. Maze, F. Jelezko, A.S. Zibrov, P.R. Hemmer, and M.D. Lukin, Quantum Register Based on Individual Electronic and Nuclear Spin Qubits in Diamond, Science, **316**, 1312 (2007).
5. A. Sipahigil, M.L. Goldman, E. Togan, Y. Chu, M. Markham, D.J. Twitchen, A.S. Zibrov, A. Kubanek, and M.D. Lukin, Quantum Interference of Single Photons from Remote Nitrogen-Vacancy Centers in Diamond, Physical Review Letters, **108**, 143601 (2012).
6. H. Bernien, L. Childress, L. Robledo, M. Markham, D. Twitchen, and R. Hanson, Two-Photon Quantum Interference from Separate Nitrogen Vacancy Centers in Diamond, Physical Review Letters, **108**, 043604 (2012).
7. P.C. Maurer, G. Kucsko, C. Latta, L. Jiang, N.Y. Yao, S.D. Bennett, F. Pastawski, D. Hunger, N. Chisholm, M. Markham, D.J. Twitchen, J.I. Cirac, and M.D. Lukin, Room-Temperature Quantum Bit Memory Exceeding One Second, Science, **336**, 1283 (2012).
8. H. Bernien, B. Hensen, W. Pfaff, G. Koolstra, M.S. Blok, L. Robledo, T.H. Taminiau, M. Markham, D.J. Twitchen, L. Childress, and R. Hanson, Heralded entanglement between solid-state qubits separated by three metres, Nature, **497**, 86 (2013).
9. W. Pfaff, B.J. Hensen, H. Bernien, S.B. van Dam, M.S. Blok, T.H. Taminiau, M.J. Tiggelman, R.N. Schouten, M. Markham, D.J. Twitchen, and R. Hanson, Unconditional quantum teleportation between distant solid-state quantum bits, Science, **345**, 532 (2014).
10. B. Hensen, H. Bernien, A.E. Dreau, A. Reiserer, N. Kalb, M.S. Blok, J. Ruitenberg, R.F.L. Vermeulen, R.N. Schouten, C. Abellan, W. Amaya, V. Pruneri, M.W. Mitchell, M. Markham, D.J. Twitchen, D. Elkouss, S. Wehner, T.H. Taminiau, and R. Hanson, Loophole-free Bell inequality violation using electron spins separated by 1.3 kilometres, Nature, **526**, 682 (2015).
11. H.J. Kimble, The quantum internet, Nature, **453**, 1023 (2008).
12. A. Sipahigil, R.E. Evans, D.D. Sukachev, M.J. Burek, J. Borregaard, M. Bhaskar, C. Nguyen, J. Pacheco, H.A. Atikian, C. Meuwly, R.M. Camacho, F. Jelezko, E. Bielejec, H. Park, M. Loncar, and M.D. Lukin, An integrated diamond nanophotonics platform for quantum-optical networks, Science, **354**, 847 (2016).
13. D.E. Chang, V. Vuletic, and M.D. Lukin, Quantum nonlinear optics - photon by photon, Nat Photon, **8**, 685 (2014).
14. B.J.M. Hausmann, B.J. Shields, Q. Quan, Y. Chu, N.P. de Leon, R. Evans, M.J. Burek, A.S. Zibrov, M. Markham, D.J. Twitchen, H. Park, M.D. Lukin, and M. Loncăr, Coupling of NV Centers to Photonic Crystal Nanobeams in Diamond, Nano Letters, **13**, 5791 (2013).
15. B.J.M. Hausmann, I.B. Bulu, P.B. Deotare, M. McCutcheon, V. Venkataraman, M.L. Markham, D.J. Twitchen, and M. Lončar, Integrated High-Quality Factor Optical Resonators in Diamond, Nano Letters, **13**, 1898 (2013).

16. A. Faraon, C. Santori, Z. Huang, V.M. Acosta, and R.G. Beausoleil, Coupling of Nitrogen-Vacancy Centers to Photonic Crystal Cavities in Monocrystalline Diamond, Physical Review Letters, **109**, 033604 (2012).
17. A. Faraon, P.E. Barclay, C. Santori, K.-M.C. Fu, and R.G. Beausoleil, Resonant enhancement of the zero-phonon emission from a colour centre in a diamond cavity, Nat Photon, **5**, 301 (2011).
18. A. Faraon, C. Santori, Z. Huang, K.-M. C. Fu, V. M. Acosta, D. Fattal, and R. G. Beausoleil, Quantum photonic devices in single-crystal diamond, New Journal of Physics, **15**, 025010 (2013).
19. J.C. Lee, D.O. Bracher, S. Cui, K. Ohno, C.A. McLellan, X. Zhang, P. Andrich, B. Alemán, K.J. Russell, A.P. Magyar, I. Aharonovich, A. Bleszynski Jayich, D. Awschalom, and E.L. Hu, Deterministic coupling of delta-doped nitrogen vacancy centers to a nanobeam photonic crystal cavity, Applied Physics Letters, **105**, 261101 (2014).
20. A.P. Magyar, J.C. Lee, A.M. Limarga, I. Aharonovich, F. Rol, D.R. Clarke, M. Huang, and E.L. Hu, Fabrication of thin, luminescent, single-crystal diamond membranes, Applied Physics Letters, **99**, 081913 (2011).
21. L. Li, T. Schröder, E.H. Chen, M. Walsh, I. Bayn, J. Goldstein, O. Gaathon, M.E. Trusheim, M. Lu, J. Mower, M. Cotlet, M.L. Markham, D.J. Twitchen, and D. Englund, Coherent spin control of a nanocavity-enhanced qubit in diamond, Nat Commun, **6**, 6173 (2015).
22. Bhaskar M. K., Sukachev D. D, Sipahigil A., Evans R. E., Burek M. J., Nguyen C. T., Rogers L. J., Siyushev P., Metsch M. H., Park H., Jelezko F., Loncar M., and L.M. D., Quantum nonlinear optics with a germanium-vacancy color center in a nanoscale diamond waveguide, Physical Review Letters, **118**, 223603 (2017).
23. J.C. Lee, I. Aharonovich, A.P. Magyar, F. Rol, and E.L. Hu, Coupling of silicon-vacancy centers to a single crystal diamond cavity, Optics Express, **20**, 8891 (2012).
24. J. Riedrich-Moller, L. Kipfstuhl, C. Hepp, E. Neu, C. Pauly, F. Mucklich, A. Baur, M. Wandt, S. Wolff, M. Fischer, S. Gsell, M. Schreck, and C. Becher, One- and two-dimensional photonic crystal microcavities in single crystal diamond, Nat Nano, **7**, 69 (2012).
25. J. Riedrich-Möller, C. Arend, C. Pauly, F. Mücklich, M. Fischer, S. Gsell, M. Schreck, and C. Becher, Deterministic Coupling of a Single Silicon-Vacancy Color Center to a Photonic Crystal Cavity in Diamond, Nano Letters, **14**, 5281 (2014).
26. Sara Mouradian, Noel H. Wan, Tim Schröder, and D. Englund, Rectangular photonic crystal nanobeam cavities in bulk diamond, arXiv:1704.07918, (2017).
27. M.J. Burek, N.P. de Leon, B.J. Shields, B.J.M. Hausmann, Y. Chu, Q. Quan, A.S. Zibrov, H. Park, M.D. Lukin, and M. Lončar, Free-Standing Mechanical and Photonic Nanostructures in Single-Crystal Diamond, Nano Letters, **12**, 6084 (2012).
28. P. Latawiec, M.J. Burek, Y.-I. Sohn, and M. Lončar, Faraday cage angled-etching of nanostructures in bulk dielectrics, Journal of Vacuum Science & Technology B, **34**, 041801 (2016).
29. H.A. Atikian, P. Latawiec, M.J. Burek, Y.-I. Sohn, S. Meesala, N. Gravel, A.B. Kouki, and M. Lončar, Freestanding nanostructures via reactive ion beam angled etching, APL Photonics, **2**, 051301 (2017).
30. I. Bayn, S. Mouradian, L. Li, J.A. Goldstein, T. Schröder, J. Zheng, E.H. Chen, O. Gaathon, M. Lu, A. Stein, C.A. Ruggiero, J. Salzman, R. Kalish, and D. Englund, Fabrication of triangular nanobeam waveguide networks in bulk diamond using single-crystal silicon hard masks, Applied Physics Letters, **105**, 211101 (2014).
31. M.J. Burek, Y. Chu, M.S.Z. Liddy, P. Patel, J. Rochman, S. Meesala, W. Hong, Q. Quan, M.D. Lukin, and M. Lončar, High quality-factor optical nanocavities in bulk single-crystal diamond, Nat Commun, **5**, 5718 (2014).

32. R.E. Evans, A. Sipahigil, D.D. Sukachev, A.S. Zibrov, and M.D. Lukin, Narrow-linewidth homogeneous optical emitters in diamond nanostructures via silicon ion implantation, Physical Review Applied, **5**, 044010 (2016).
33. Y. Chu, N.P. de Leon, B.J. Shields, B. Hausmann, R. Evans, E. Togan, M.J. Burek, M. Markham, A. Stacey, A.S. Zibrov, A. Yacoby, D.J. Twitchen, M. Loncar, H. Park, P. Maletinsky, and M.D. Lukin, Coherent Optical Transitions in Implanted Nitrogen Vacancy Centers, Nano Letters, **14**, 1982 (2014).
34. P. Latawiec, V. Venkataraman, M.J. Burek, B.J.M. Hausmann, I. Bulu, and M. Lončar, On-chip diamond Raman laser, Optica, **2**, 924 (2015).
35. B.J.M. Hausmann, I. Bulu, V. Venkataraman, P. Deotare, and M. Loncar, Diamond nonlinear photonics, Nat Photon, **8**, 369 (2014).
36. M.J. Burek, J.D. Cohen, S.M. Meenehan, N. El-Sawah, C. Chia, T. Ruelle, S. Meesala, J. Rochman, H.A. Atikian, M. Markham, D.J. Twitchen, M.D. Lukin, O. Painter, and M. Lončar, Diamond optomechanical crystals, Optica, **3**, 1404 (2016).
37. M. Mitchell, B. Khanaliloo, D.P. Lake, T. Masuda, J.P. Hadden, and P.E. Barclay, Single-crystal diamond low-dissipation cavity optomechanics, Optica, **3**, 963 (2016).
38. S.L. Mouradian, T. Schröder, C.B. Poitras, L. Li, J. Goldstein, E.H. Chen, M. Walsh, J. Cardenas, M.L. Markham, D.J. Twitchen, M. Lipson, and D. Englund, Scalable Integration of Long-Lived Quantum Memories into a Photonic Circuit, Physical Review X, **5**, 031009 (2015).
39. T.G. Tiecke, K.P. Nayak, J.D. Thompson, T. Peyronel, N.P. de Leon, V. Vuletić, and M.D. Lukin, Efficient fiber-optical interface for nanophotonic devices, Optica, **2**, 70 (2015).
40. S. Gröblacher, J.T. Hill, A.H. Safavi-Naeini, J. Chan, and O. Painter, Highly efficient coupling from an optical fiber to a nanoscale silicon optomechanical cavity, Applied Physics Letters, **103**, 181104 (2013).
41. R.S. Daveau, K.C. Balram, T. Pregnolato, J. Liu, E.H. Lee, J.D. Song, V. Verma, R. Mirin, S.W. Nam, L. Midolo, S. Stobbe, K. Srinivasan, and P. Lodahl, Efficient fiber-coupled single-photon source based on quantum dots in a photonic-crystal waveguide, Optica, **4**, 178 (2017).
42. R.N. Patel, T. Schroder, N. Wan, L. Li, S.L. Mouradian, E.H. Chen, and D.R. Englund, Efficient photon coupling from a diamond nitrogen vacancy center by integration with silica fiber, Light Sci Appl, **5**, e16032 (2016).
43. M.J. Burek and M. Loncar, US Patent App. 13/954,108, *Device support structures from bulk substrates*, (2015).
44. A. Sipahigil, K.D. Jahnke, L.J. Rogers, T. Teraji, J. Isoya, A.S. Zibrov, F. Jelezko, and M.D. Lukin, Indistinguishable Photons from Separated Silicon-Vacancy Centers in Diamond, Physical Review Letters, **113**, 113602 (2014).
45. See Supplementary Material for additional details.
46. P.B. Deotare, M.W. McCutcheon, I.W. Frank, M. Khan, and M. Lončar, High quality factor photonic crystal nanobeam cavities, Applied Physics Letters, **94**, 121106 (2009).
47. Q. Quan, P.B. Deotare, and M. Loncar, Photonic crystal nanobeam cavity strongly coupled to the feeding waveguide, Applied Physics Letters, **96**, 203102 (2010).
48. J.D. Joannopoulos, S.G. Johnson, J.N. Winn, and R.D. Meade, *Photonic Crystals: Molding the Flow of Light, 2nd ed*. 2008: Princeton University Press.
49. L.J. Rogers, K.D. Jahnke, M.W. Doherty, A. Dietrich, L.P. McGuinness, C. Müller, T. Teraji, H. Sumiya, J. Isoya, N.B. Manson, and F. Jelezko, Electronic structure of the negatively charged silicon-vacancy center in diamond, Physical Review B, **89**, 235101 (2014).
50. C. Hepp, T. Müller, V. Waselowski, J.N. Becker, B. Pingault, H. Sternschulte, D. Steinmüller-Nethl, A. Gali, J.R. Maze, M. Atatüre, and C. Becher, Electronic Structure of the Silicon Vacancy Color Center in Diamond, Physical Review Letters, **112**, 036405 (2014).

51. C. Sauvan, G. Lecamp, P. Lalanne, and J.P. Hugonin, Modal-reflectivity enhancement by geometry tuning in Photonic Crystal microcavities, Optics Express, **13**, 245 (2005).
52. D.R. Turner, US Patent 4,469,554, *Etch procedure for optical fibers*, (1984).
53. T. Schröder, M. E. Trusheim, M. Walsh, L. Li, J. Zheng, M. Schukraft, J.L. Pacheco, R.M. Camacho, E.S. Bielejec, A. Sipahigil, R.E. Evans, D.D. Sukachev, C.T. Nguyen, M.D. Lukin, and D. Englund, Scalable focused ion beam creation of nearly lifetime-limited single quantum emitters in diamond nanostructures, Nature Communications, **8**, 15376 (2017).
54. T. Syuto, K. Godai, K. Akira, T. Tokuyuki, O. Shinobu, P.M. Liam, R. Lachlan, N. Boris, E. Wu, Y. Liu, J. Fedor, O. Takeshi, I. Junichi, S. Takahiro, and T. Takashi, Array of bright silicon-vacancy centers in diamond fabricated by low-energy focused ion beam implantation, Applied Physics Express, **7**, 115201 (2014).
55. K.D. Jahnke, A. Sipahigil, J.M. Binder, M.W. Doherty, M. Metsch, L.J. Rogers, N.B. Manson, M.D. Lukin, and F. Jelezko, Electron–phonon processes of the silicon-vacancy centre in diamond, New Journal of Physics, **17**, 043011 (2015).
56. L. Li, E.H. Chen, J. Zheng, S.L. Mouradian, F. Dolde, T. Schröder, S. Karaveli, M.L. Markham, D.J. Twitchen, and D. Englund, Efficient Photon Collection from a Nitrogen Vacancy Center in a Circular Bullseye Grating, Nano Letters, **15**, 1493 (2015).
57. J.N. Becker, J. Görlitz, C. Arend, M. Markham, and C. Becher, Ultrafast all-optical coherent control of single silicon vacancy colour centres in diamond, Nature Communications, **7**, 13512 (2016).
58. L.J. Rogers, K.D. Jahnke, M.H. Metsch, A. Sipahigil, J.M. Binder, T. Teraji, H. Sumiya, J. Isoya, M.D. Lukin, P. Hemmer, and F. Jelezko, All-Optical Initialization, Readout, and Coherent Preparation of Single Silicon-Vacancy Spins in Diamond, Physical Review Letters, **113**, 263602 (2014).
59. B. Pingault, J.N. Becker, C.H.H. Schulte, C. Arend, C. Hepp, T. Godde, A.I. Tartakovskii, M. Markham, C. Becher, and M. Atatüre, All-Optical Formation of Coherent Dark States of Silicon-Vacancy Spins in Diamond, Physical Review Letters, **113**, 263601 (2014).

FIGURES

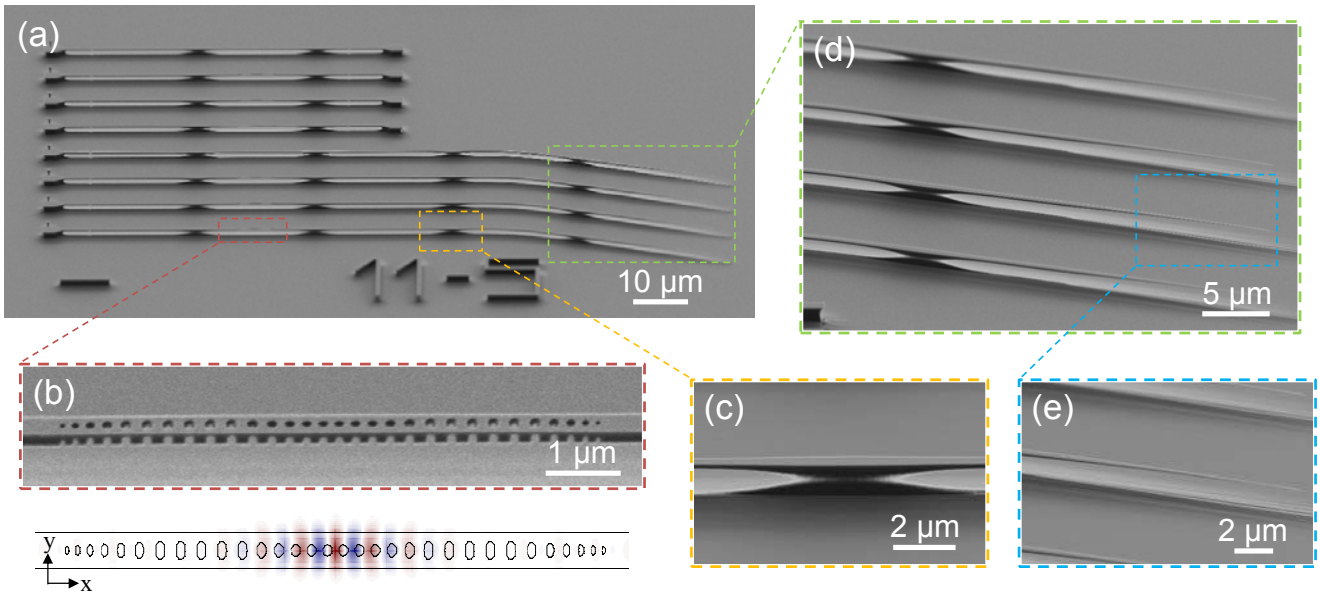

Figure 1 | On-chip diamond nanophotonic structures. SEM images of (a) an array of diamond nanophotonic structures, fabricated using angled-etching techniques [45]. The four key components in each device are: (1) freestanding diamond waveguides, (2) integrated diamond nanobeam photonic crystal cavities (panels (b) with the top down electric field profile of the fundamental optical cavity mode inset), (3) vertical waveguide support structures (panel (c)), and lastly, (4) freestanding diamond waveguide tapers (panels (d) and (e)).

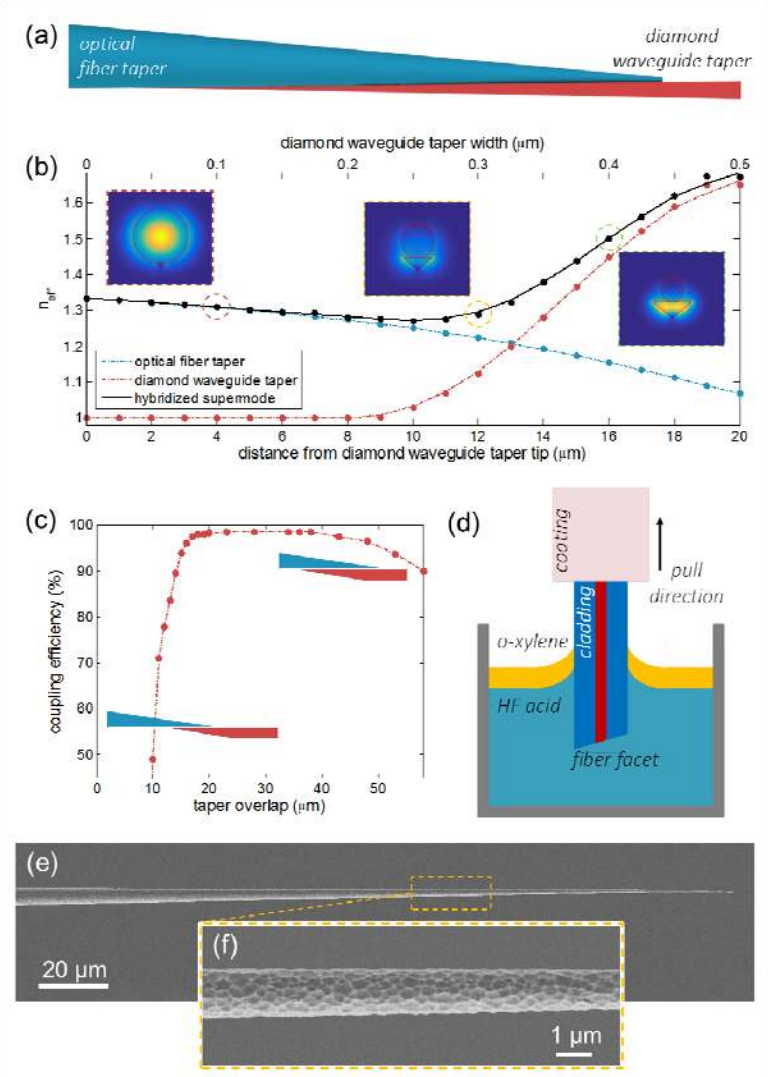

Figure 2 | Single-mode optical fiber taper fabrication. (a) Schematic of fiber-waveguide taper adiabatic coupling. The single-ended conical optical fiber taper (OFT, blue) is physically contacted with a diamond waveguide taper (DWT, red). (b) Effective indices (n_{eff}, calculated via an eigenmode solver) of the OFT and transverse-electric (TE) polarized DWT modes for taper angle of 1.5° in both cases. Inset: cross-sectional energy density profile ($|E|^2$) obtained from eigenmode simulations at the indicated points along the physically overlapped tapers. (c) Simulated coupling efficiencies for transmission from the fundamental diamond TE-polarized waveguide mode to the optical fiber HE_{11} mode as a function of fiber-waveguide taper overlap for a 20 μm long DWT. (d) Schematic of fabrication of single-ended conical OFTs by hydrofluoric acid etching. (e) SEM image of a fabricated OFT tip, with (f) a zoomed in image of the chemically etched surface roughness.

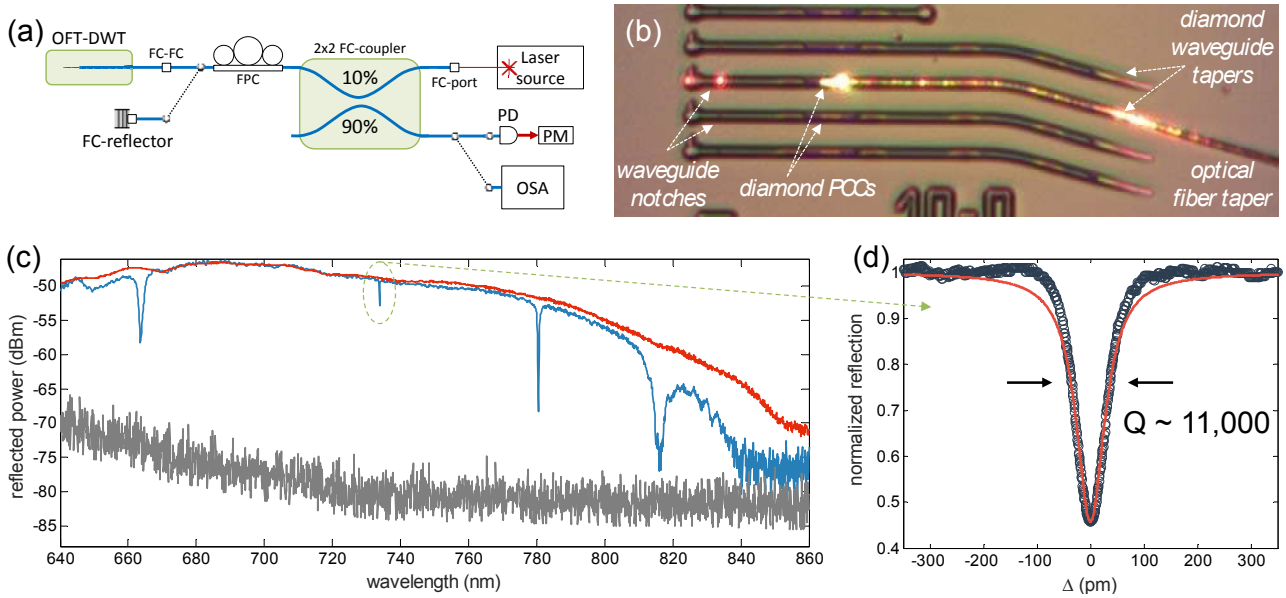

Figure 3 | Optical characterization of diamond nanophotonic structures. (a) Schematic of the visible band fiber optical characterization set up. (b) Optical micrograph of a single-ended optical fiber taper (OFT) in contact with a diamond waveguide taper (DWT) under white light illumination. (c) Broadband reflection spectra of diamond photonic crystal cavity (PCC, blue curve) and a commercial fiber-coupled retroreflector (red curve). The noise floor of the optical spectrum analyzer (OSA) is shown in grey. (d) Normalized high resolution spectrum of the fundamental diamond nanobeam PCC mode centered at $\lambda \sim 733.9$ nm. A Lorentzian fit (red curve) yields a Q-factor estimate of $Q \sim 1.1 \times 10^4$.

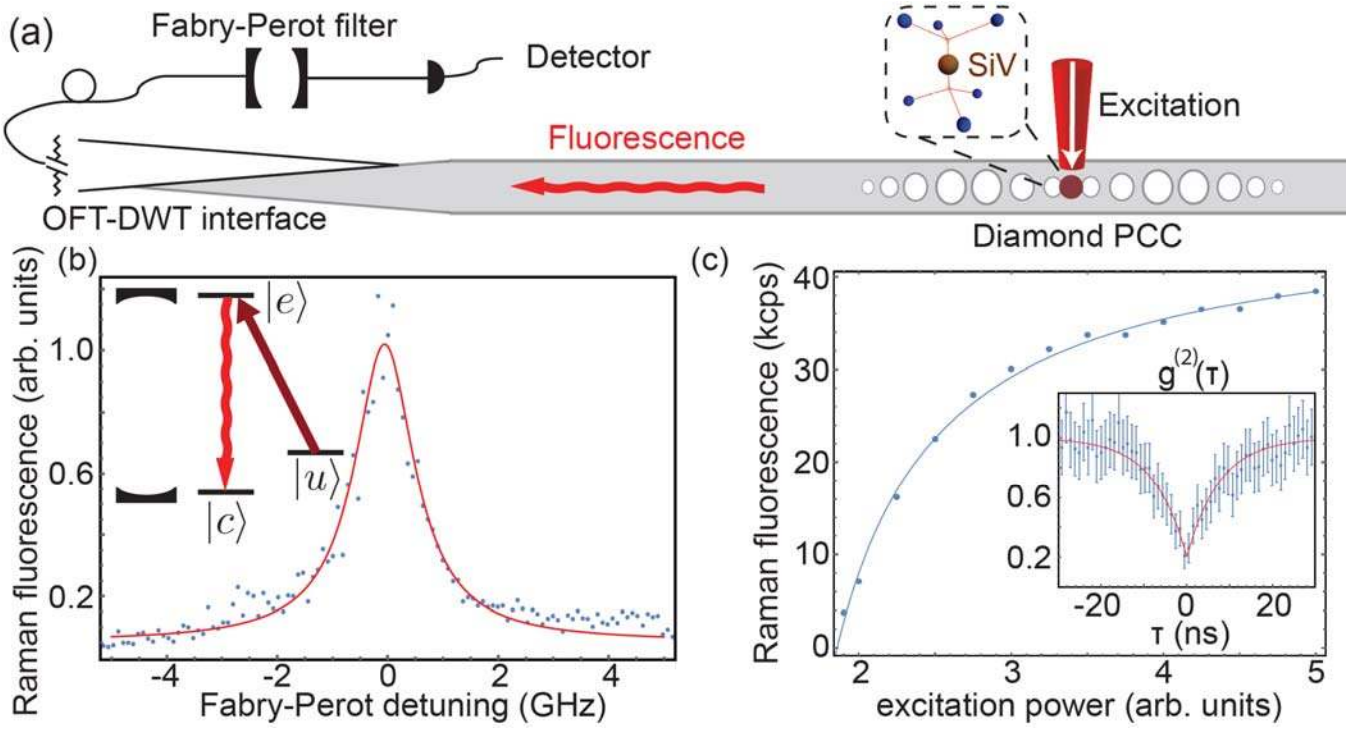

Figure 4 | Efficient generation and collection of narrowband single photons. (a) A diamond SiV color center embedded inside a diamond photonic crystal cavity (PCC) is excited from free space, and fluorescence in the diamond waveguide is collected into the optical fiber taper. A Fabry-Perot (FP) cavity is used to measure the spectrum of the emitted photons. (b) Spectrum of collected photons. The excitation laser is resonant with the |*u*> to |*e*> transition. The transmitted Raman fluorescence is recorded as the resonance frequency of the FP cavity is scanned across the |e> to |c> transition to obtain an upper bound on the linewidth of detected photons of 1.27 +/- 0.20 GHz. (c) Saturation measurement of Raman photons with the PCC resonant with the |e> to |c> transition. We subtract the linear background set by the excitation laser, detecting a narrow-band single photon flux of at least 38 kHz when the PCC is on resonance. Inset: anti-bunching of $g^{(2)}(0) = 0.21 +/- 0.09$ in the Raman fluorescence autocorrelation confirms the generation of single photons.